

Partial-wave analysis of $\pi^-p \rightarrow \eta n$ and $\pi^-p \rightarrow K^0\Lambda$ reactions

M. Shrestha¹ and D. M. Manley¹

¹*Department of Physics, Kent State University, Kent, OH 44242-0001*

Abstract

We investigate the hadronic reactions $\pi N \rightarrow \eta N$ and $\pi N \rightarrow K\Lambda$ via single-energy partial-wave analyses in the c.m. energy range 1080 to 2100 MeV. Our results for the $K\Lambda$ channel are consistent with prior works; however, for the ηN channel our results differ significantly from previous energy-dependent partial-wave analyses that violate the S -matrix unitarity. We present the first (new) results of ηN and $K\Lambda$ partial-wave amplitudes constrained by a unitary energy-dependent model. We obtain excellent predictions of integrated cross sections for the two reactions from a global energy-dependent solution. Our results imply that the region just above $S_{11}(1535)$ has a major contribution from $P_{11}(1710)$ for $\pi^-p \rightarrow \eta n$, whereas the large peak near 1700 MeV in $\pi^-p \rightarrow K^0\Lambda$ is dominated by contributions from both $S_{11}(1650)$ and $P_{11}(1710)$.

PACS numbers: 13.75.Gx; 14.20.Gk

I. INTRODUCTION AND MOTIVATION

The importance of the hadronic reactions $\pi N \rightarrow \eta N$ and $\pi N \rightarrow K\Lambda$ cannot be overstated. The huge amount of high-quality data on the electromagnetic processes $\gamma N \rightarrow \eta N$ and $\gamma N \rightarrow K\Lambda$ from various facilities (ELSA, GRAAL, JLAB, LEPS, MAMI), when analyzed and interpreted by phenomenologists, will certainly lead to a clearer picture of the baryon resonance spectrum. The validity of resonance parameters thus extracted will not be substantiated without similar results from studies of the corresponding hadronic reactions. The study of $\pi N \rightarrow \eta N$ and $\pi N \rightarrow K\Lambda$ complements the study of eta and kaon photoproduction.

Most previous partial-wave analyses (PWAs) of $\pi^- p \rightarrow \eta n$ [1, 2] and $\pi^- p \rightarrow K^0 \Lambda$ [3–6] were based on the assumption that partial-wave amplitudes could be represented by a simple sum of resonant and background terms. Such an assumption violates unitarity of the partial-wave S -matrix. In this work, we report on our investigation of the reactions $\pi^- p \rightarrow \eta n$ and $\pi^- p \rightarrow K^0 \Lambda$ via single-energy analyses. All available differential cross section, polarization, polarized cross section, and spin-rotation data within the energy limits of this analysis were fitted. In order to ensure that our amplitudes had a relatively smooth variation with energy, we introduced several constraints that will be described in detail below.

II. FORMALISM AND FITTING PROCEDURES

Here, we summarize the formalism for the single-energy partial-wave analyses. The data were analyzed in small energy bins. Within each energy bin, each amplitude was approximated as a complex constant. The differential cross section $d\sigma/d\Omega$ and polarization P are given by

$$\frac{d\sigma}{d\Omega} = \lambda^2(|f|^2 + |g|^2), \quad (1)$$

$$P \frac{d\sigma}{d\Omega} = 2\lambda^2 \text{Im}(fg^*), \quad (2)$$

where $\lambda = \hbar/k$, with k the magnitude of c.m. momentum of the incoming particle. In addition, the spin-rotation parameter is defined by

$$\beta = \arg \left(\frac{f - ig}{f + ig} \right), \quad (3)$$

from which it follows that

$$\beta = \tan^{-1} \left(\frac{-2\text{Re}(f^*g)}{|f|^2 - |g|^2} \right). \quad (4)$$

Here, $f = f(W, \theta)$ and $g = g(W, \theta)$ are the usual spin-non-flip and spin-flip amplitudes at c.m. energy W and meson c.m. scattering angle θ . In terms of partial waves, f and g can be expanded as

$$f(W, \theta) = \sum_{l=0}^{\infty} [(l+1)T_{l+} + lT_{l-}] P_l(\cos \theta), \quad (5)$$

$$g(W, \theta) = \sum_{l=1}^{\infty} [T_{l+} - T_{l-}] P_l^1(\cos \theta), \quad (6)$$

where l is the initial orbital angular momentum, $P_l(\cos \theta)$ is a Legendre polynomial and $P_l^1(\cos \theta) = \sin \theta \cdot dP_l(\cos \theta)/d(\cos \theta)$. The total angular momentum for the amplitude T_{l+} is $J = l + \frac{1}{2}$, while that for the amplitude T_{l-} is $J = l - \frac{1}{2}$. For the initial πN system, we have $I = 1/2$ or $I = 3/2$ so that the amplitudes $T_{l\pm}$ can be expanded in terms of isospin amplitudes as

$$T_{l\pm} = C_{\frac{1}{2}} T_{l\pm}^{\frac{1}{2}} + C_{\frac{3}{2}} T_{l\pm}^{\frac{3}{2}}, \quad (7)$$

where $T_{l\pm}^I$ are partial-wave amplitudes with isospin I and total angular momentum $J = l \pm \frac{1}{2}$ with C_I the appropriate isospin Clebsch-Gordon coefficients for a given reaction. For $\pi^- p \rightarrow \eta n$ and $\pi^- p \rightarrow K^0 \Lambda$, we have $C_{\frac{1}{2}} = -\sqrt{\frac{2}{3}}$ and $C_{\frac{3}{2}} = 0$.

Single-energy fits were performed separately for the two reactions $\pi^- p \rightarrow \eta n$ and $\pi^- p \rightarrow K^0 \Lambda$. In each case the available data were analyzed in c.m. energy bins of width 30 MeV. This choice of bin width was appropriate because the data for smaller widths had unacceptably low statistics and for larger widths, some amplitudes varied too much to approximate them as constants over the energy spread of the bin.

Tables I and II summarize the available quantity and types of data in each energy bin for the two inelastic reactions. Spin-rotation-parameter data were available only for $\pi^- p \rightarrow K^0 \Lambda$ and no data at all were available for $\pi^- p \rightarrow \eta n$ in the bins centered at $W = 1740, 1800, 1950,$ and 2040 MeV.

From Eqs. 1 to 4 it is clear that the amplitudes f and g can be multiplied by an arbitrary phase factor without changing the corresponding observables. This feature is referred to

TABLE I. Statistics for single-energy fits for $\pi^- p \rightarrow \eta n$.

$W(\text{MeV})$	$d\sigma/d\Omega$	P	References
1530 ± 15	89	–	[1, 10, 11, 13]
1560 ± 15	47	–	[11, 12, 14]
1590 ± 15	43	–	[11–13]
1620 ± 15	28	–	[11, 13]
1650 ± 15	15	–	[11, 14]
1680 ± 15	45	–	[11, 14]
1710 ± 15	18	–	[14]
1740 ± 15	–	–	
1770 ± 15	19	5	[2, 14]
1800 ± 15	–	–	
1830 ± 15	19	5	[2, 14]
1860 ± 15	20	7	[2, 14]
1890 ± 15	20	6	[2, 14]
1920 ± 15	20	7	[2, 14]
1950 ± 15	–	–	
1980 ± 15	20	7	[2, 14]
2010 ± 15	20	7	[2, 14]
2040 ± 15	–	–	
2070 ± 15	20	7	[2, 14]

as the over-all phase ambiguity. For $\pi^- p \rightarrow \eta n$, the S_{11} amplitudes below $K\Lambda$ threshold were held fixed at the values taken from the GWU solution (SP06) [8]. This constraint also removed the over-all phase ambiguity for the ηn amplitudes below 1.6 GeV. At higher energies, the phase ambiguity for ηn amplitudes was resolved by requiring the G_{17} amplitude to have the same phase as the G_{17} elastic amplitude. For $\pi^- p \rightarrow K^0\Lambda$, plots of $|T|^2$ vs. W were made for all the contributing partial waves. The plot for the S_{11} amplitude (Fig. 1) suggested a resonant behavior near 1.65 GeV where there is the well-established $S_{11}(1650)$ resonance. The over-all phase problem for $K\Lambda$ amplitudes was thus resolved by rotating

TABLE II. Statistics for single-energy fits for $\pi^- p \rightarrow K^0 \Lambda$.

$W(\text{MeV})$	$d\sigma/d\Omega$	P	$Pd\sigma/d\Omega$	β	References
1618 ± 15	25	5	10	–	[3, 4]
1648 ± 15	30	10	10	–	[3, 4]
1678 ± 15	170	10	80	–	[3, 4]
1708 ± 15	90	10	40	–	[3, 4]
1738 ± 15	30	14	10	–	[3, 4]
1768 ± 15	10	14	–	–	[4]
1798 ± 15	10	14	–	–	[4]
1828 ± 15	10	14	–	–	[4]
1858 ± 15	10	14	–	11	[4, 6]
1888 ± 15	20	20	–	–	[5]
1918 ± 15	33	20	11	–	[5, 15]
1948 ± 15	20	20	–	9	[5, 6]
1978 ± 15	33	20	11	–	[5, 15]
2008 ± 15	19	20	–	–	[5]
2038 ± 15	33	19	11	10	[5, 6, 15]
2068 ± 15	20	18	–	11	[5, 6]

the amplitudes by a phase angle such that the rotated S_{11} amplitude had a resonant phase consistent with our prior determinations of the $S_{11}(1650)$ mass and width.

In our initial fits, the single-energy solutions described the observables extremely well but with somewhat noisy amplitudes. These amplitudes were incorporated into a global multichannel energy-dependent fit that yielded energy-dependent amplitudes consistent with two-body S -matrix unitarity. Details of the multichannel analysis will be presented in a separate publication [9]. The initial energy-dependent amplitudes failed to reproduce the $\pi^- p \rightarrow \eta n$ and $\pi^- p \rightarrow K^0 \Lambda$ observables satisfactorily so we iterated the single-energy fits.

Initially, for $K\Lambda$, only the S_{11} amplitude was fitted well with the energy-dependent fit so in the second round of single-energy fits, the S_{11} amplitude was held fixed at the energy-dependent values while the other partial-wave amplitudes were varied. The resulting con-

strained single-energy fits still gave a very good description of the observables so we used this solution in the subsequent global energy-dependent fits. This time around the P_{11} amplitude was fitted well. In the next round of single-energy fits, both the S_{11} and P_{11} amplitudes were held fixed at their energy-dependent values while the other amplitudes were varied.

Similarly, for the second iteration of the ηN analysis, the S_{11} and P_{11} amplitudes were held fixed at their respective energy-dependent values while the other amplitudes were varied. In the final iteration, the S_{11} , P_{11} and P_{13} amplitudes were held fixed, while the other amplitudes were varied.

Our initial fits indicated that the D_{13} amplitudes were not needed for either the $K\Lambda$ or the ηN fits. Thus the D_{13} amplitudes were not included in our final single-energy solutions. This is consistent with the prior work that shows the inelasticity in D_{13} is saturated by $\pi\pi N$ channels [7].

III. RESULTS AND DISCUSSION

The final single-energy fits resulted in a fairly smooth set of partial-wave amplitudes within the energy range of our analysis. Tables III and IV list the real and imaginary parts of the amplitudes tabulated against the central bin energies. The values in these tables represent the final single-energy solutions that were used as input into our subsequent global energy-dependent fits for given partial waves.

TABLE III. Partial-wave amplitudes for $\pi N \rightarrow \eta N$.

W (MeV)	S_{11}		P_{11}		P_{13}	
	$\text{Re}(S_{11})$	$\text{Im}(S_{11})$	$\text{Re}(P_{11})$	$\text{Im}(P_{11})$	$\text{Re}(P_{13})$	$\text{Im}(P_{13})$
1530			-0.018 ± 0.025	0.014 ± 0.025	-0.000 ± 0.063	-0.004 ± 0.005
1560			-0.043 ± 0.028	-0.020 ± 0.022	-0.005 ± 0.040	0.004 ± 0.023
1590			-0.063 ± 0.018	0.060 ± 0.016	-0.106 ± 0.012	-0.065 ± 0.019
1620	-0.200 ± 0.033	0.156 ± 0.040	-0.125 ± 0.036	-0.025 ± 0.037	-0.024 ± 0.017	-0.004 ± 0.036
1650	-0.218 ± 0.061	0.130 ± 0.057	-0.122 ± 0.060	-0.026 ± 0.058	-0.002 ± 0.021	-0.000 ± 0.032
1680	-0.051 ± 0.039	-0.205 ± 0.038	0.051 ± 0.039	-0.122 ± 0.030	-0.008 ± 0.027	-0.023 ± 0.030
1710	-0.042 ± 0.046	-0.225 ± 0.037	0.039 ± 0.049	-0.197 ± 0.036	0.058 ± 0.037	0.013 ± 0.041
1770	-0.033 ± 0.043	-0.197 ± 0.023	0.044 ± 0.046	-0.193 ± 0.030	0.021 ± 0.024	0.028 ± 0.028
1830	0.196 ± 0.035	0.143 ± 0.041	0.120 ± 0.038	0.144 ± 0.034	0.047 ± 0.022	0.020 ± 0.029
1860	0.181 ± 0.019	0.160 ± 0.023	0.091 ± 0.022	0.207 ± 0.020	0.074 ± 0.026	0.003 ± 0.019
1890	0.192 ± 0.025	0.140 ± 0.031	0.077 ± 0.025	0.169 ± 0.024	0.063 ± 0.016	0.003 ± 0.017
1920	0.158 ± 0.036	0.131 ± 0.041	0.056 ± 0.033	0.153 ± 0.032	0.066 ± 0.026	0.001 ± 0.017
1980	0.138 ± 0.054	0.143 ± 0.057	0.027 ± 0.042	0.114 ± 0.042	0.047 ± 0.041	0.082 ± 0.041
2010	0.112 ± 0.059	0.128 ± 0.062	0.019 ± 0.043	0.063 ± 0.035	0.072 ± 0.039	0.052 ± 0.035
2070	0.089 ± 0.047	0.156 ± 0.048	-0.008 ± 0.030	0.092 ± 0.025	0.084 ± 0.033	0.098 ± 0.027

Figure 2 shows representative final single-energy fits for the $\pi^- p \rightarrow \eta n$ differential cross section for bins centered at $W = 1530, 1590, 1680, 1770, 1890,$ and 2010 MeV. The first three panels of Fig. 2 reveal an inconsistency in the data over the small variation in c.m. energy within the bin. Note that in these panels, there are data from the same references (Brown *et al.* [14] and Debehm *et al.* [11]) at two or more slightly different energies. Our single-energy analysis gives a weighted average fit to the data sets. Figure 3 similarly shows final single-energy fits for the reaction $\pi^- p \rightarrow K^0 \Lambda$ differential cross section for bins centered at $W = 1648, 1738, 1828, 1918, 1978,$ and 2038 MeV. Figure 4 shows final single-energy fits for the spin rotation parameter for $\pi^- p \rightarrow K^0 \Lambda$. In general, our final results are in very good agreement with the available data.

TABLE III. Continued.

W (MeV)	D_{15}		F_{15}		G_{17}	
	Re(D_{15})	Im(D_{15})	Re(F_{15})	Im(F_{15})	Re(G_{17})	Im(G_{17})
1530	0.007 ± 0.015	0.013 ± 0.002				
1560	0.002 ± 0.022	0.035 ± 0.008				
1590	0.041 ± 0.011	0.086 ± 0.003				
1620	-0.031 ± 0.016	0.032 ± 0.034	0.042 ± 0.017	-0.023 ± 0.034		
1650	-0.040 ± 0.030	0.005 ± 0.024	0.044 ± 0.030	0.020 ± 0.023		
1680	-0.054 ± 0.030	0.024 ± 0.037	0.033 ± 0.030	0.014 ± 0.037		
1710	-0.001 ± 0.029	-0.023 ± 0.030	-0.045 ± 0.026	0.056 ± 0.032	-0.035 ± 0.024	0.031 ± 0.024
1770	0.039 ± 0.015	0.007 ± 0.021	-0.094 ± 0.012	-0.000 ± 0.026	-0.041 ± 0.021	-0.041 ± 0.021
1830	-0.011 ± 0.021	-0.001 ± 0.021	-0.042 ± 0.027	-0.052 ± 0.024	-0.027 ± 0.016	-0.038 ± 0.016
1860	-0.005 ± 0.011	0.032 ± 0.009	-0.085 ± 0.010	-0.047 ± 0.012	-0.037 ± 0.010	-0.017 ± 0.010
1890	-0.031 ± 0.010	0.018 ± 0.014	-0.044 ± 0.013	-0.050 ± 0.012	-0.060 ± 0.009	-0.029 ± 0.009
1920	-0.047 ± 0.011	0.023 ± 0.013	-0.046 ± 0.017	-0.054 ± 0.015	-0.042 ± 0.010	-0.030 ± 0.010
1980	-0.024 ± 0.026	-0.011 ± 0.023	-0.034 ± 0.027	-0.066 ± 0.020	-0.054 ± 0.022	-0.064 ± 0.022
2010	0.016 ± 0.032	-0.009 ± 0.022	-0.027 ± 0.034	-0.045 ± 0.014	-0.021 ± 0.026	-0.060 ± 0.026
2070	0.040 ± 0.019	-0.011 ± 0.012	-0.035 ± 0.024	-0.076 ± 0.011	-0.024 ± 0.019	-0.071 ± 0.019

Figure 5 shows our predictions for the integrated cross sections for the two inelastic reactions obtained using our energy-dependent amplitudes. In the threshold region for $\pi^- p \rightarrow \eta n$, the different data do not agree well with each other but our prediction is in excellent agreement with the latest and more precise data by Prakhov *et al.* [10]. Figure 5 also shows the individual contributions from the dominant partial waves. From this breakdown, it is clear that the S_{11} amplitude (red curve) dominates the peak region associated with the $S_{11}(1535)$ resonance. However, the contribution from S_{11} is small in the vicinity of the $S_{11}(1650)$. The next important partial wave is P_{11} with a peak around 1700 MeV as shown by the brown curve. The contributions from other partial waves are small. Also one can see a small cusp effect on the blue curve (KSU prediction) near 1620 MeV that indicates

TABLE IV. Partial-wave amplitudes for $\pi N \rightarrow K\Lambda$.

W (MeV)	S_{11}		P_{11}		P_{13}	
	$\text{Re}(S_{11})$	$\text{Im}(S_{11})$	$\text{Re}(P_{11})$	$\text{Im}(P_{11})$	$\text{Re}(P_{13})$	$\text{Im}(P_{13})$
1618	-0.065 ± 0.003	-0.085 ± 0.003	0.047 ± 0.007	-0.067 ± 0.008	0.006 ± 0.005	0.006 ± 0.015
1648	-0.052 ± 0.003	-0.169 ± 0.010	0.073 ± 0.007	-0.096 ± 0.003	-0.008 ± 0.006	-0.003 ± 0.005
1678	0.028 ± 0.003	-0.186 ± 0.017	0.118 ± 0.004	-0.093 ± 0.005	-0.029 ± 0.005	-0.035 ± 0.003
1708	0.097 ± 0.009	-0.158 ± 0.015	0.152 ± 0.011	0.025 ± 0.016	-0.011 ± 0.007	-0.061 ± 0.006
1738	0.120 ± 0.014	-0.113 ± 0.013	0.153 ± 0.017	0.025 ± 0.029	-0.017 ± 0.008	-0.062 ± 0.008
1768	0.129 ± 0.014	-0.085 ± 0.009	0.123 ± 0.022	0.082 ± 0.023	-0.002 ± 0.007	-0.061 ± 0.006
1798	0.130 ± 0.014	-0.065 ± 0.007	0.106 ± 0.025	0.129 ± 0.023	-0.018 ± 0.008	-0.071 ± 0.010
1828	0.096 ± 0.013	-0.039 ± 0.005	0.062 ± 0.022	0.050 ± 0.014	0.007 ± 0.009	-0.028 ± 0.009
1858	0.139 ± 0.008	-0.048 ± 0.003	0.068 ± 0.010	0.064 ± 0.013	0.022 ± 0.011	-0.045 ± 0.006
1888	0.110 ± 0.014	-0.033 ± 0.004	0.072 ± 0.016	0.070 ± 0.020	-0.002 ± 0.012	-0.080 ± 0.008
1918	0.109 ± 0.014	-0.029 ± 0.004	0.077 ± 0.024	0.057 ± 0.020	0.043 ± 0.018	-0.099 ± 0.011
1948	0.060 ± 0.013	-0.014 ± 0.003	0.086 ± 0.016	0.062 ± 0.013	0.026 ± 0.010	-0.037 ± 0.008
1978	0.091 ± 0.014	-0.019 ± 0.003	0.036 ± 0.018	0.032 ± 0.010	0.039 ± 0.019	-0.002 ± 0.011
2008	0.081 ± 0.020	-0.016 ± 0.004	0.063 ± 0.018	0.023 ± 0.021	0.028 ± 0.015	-0.007 ± 0.013
2038	0.061 ± 0.022	-0.011 ± 0.004	0.072 ± 0.012	0.034 ± 0.027	0.019 ± 0.014	0.004 ± 0.010
2068	0.066 ± 0.014	-0.011 ± 0.002	0.071 ± 0.011	0.032 ± 0.019	0.031 ± 0.008	-0.017 ± 0.013

the opening of the $K\Lambda$ channel. For $\pi^- p \rightarrow K^0\Lambda$, the peak near 1700 MeV is described by almost equal contributions from the S_{11} and P_{11} partial waves, which suggests considerable $K\Lambda$ coupling to the $S_{11}(1650)$ and $P_{11}(1710)$ resonances. The P_{13} partial wave (black curve) contributes to the small suggested peak near 1900 MeV. This feature is consistent with a prominent peak seen near 1900 MeV in the reaction $\gamma p \rightarrow K^+\Lambda$ [18].

Early analyses of $\pi^- p \rightarrow \eta n$ were energy-dependent PWAs based on a simple assumption that the partial-wave amplitudes could be parameterized as either $T = T_B + T_R$ [1] or $T = T_R$ without a background term [2]. The 1975 analysis by Feltesse *et al.* [1] used far fewer data than the 1979 analysis by Baker *et al.* [2], which included polarization data unlike

TABLE IV. Continued.

W (MeV)	D_{15}		F_{15}		F_{17}	
	$\text{Re}(D_{15})$	$\text{Im}(D_{15})$	$\text{Re}(F_{15})$	$\text{Im}(F_{15})$	$\text{Re}(F_{17})$	$\text{Im}(F_{17})$
1618	-0.014 ± 0.006	0.032 ± 0.005	-0.010 ± 0.009	-0.011 ± 0.004		
1648	-0.013 ± 0.007	0.006 ± 0.008	-0.009 ± 0.009	-0.012 ± 0.008		
1678	-0.006 ± 0.006	-0.001 ± 0.005	0.016 ± 0.009	-0.011 ± 0.007		
1708	-0.009 ± 0.007	0.003 ± 0.006	0.025 ± 0.011	-0.008 ± 0.016		
1738	-0.023 ± 0.008	-0.018 ± 0.011	0.027 ± 0.012	-0.007 ± 0.017		
1768	-0.006 ± 0.010	-0.024 ± 0.011	0.010 ± 0.010	0.003 ± 0.009		
1798	-0.009 ± 0.012	-0.033 ± 0.010	0.021 ± 0.017	0.003 ± 0.014		
1828	-0.001 ± 0.017	-0.026 ± 0.016	0.006 ± 0.016	0.014 ± 0.016		
1858	-0.018 ± 0.009	-0.059 ± 0.006	0.004 ± 0.008	-0.024 ± 0.008	0.005 ± 0.008	-0.014 ± 0.006
1888	0.007 ± 0.008	-0.067 ± 0.007	0.011 ± 0.008	-0.009 ± 0.009	-0.009 ± 0.008	-0.003 ± 0.008
1918	0.023 ± 0.008	-0.086 ± 0.016	0.009 ± 0.007	-0.011 ± 0.007	-0.010 ± 0.007	-0.001 ± 0.005
1948	-0.022 ± 0.010	-0.080 ± 0.007	-0.003 ± 0.014	-0.024 ± 0.008	-0.003 ± 0.006	-0.008 ± 0.005
1978	-0.022 ± 0.012	-0.073 ± 0.007	0.007 ± 0.007	-0.007 ± 0.008	-0.005 ± 0.005	-0.008 ± 0.004
2008	0.011 ± 0.013	-0.066 ± 0.007	-0.014 ± 0.009	-0.004 ± 0.008	0.010 ± 0.008	-0.011 ± 0.008
2038	0.003 ± 0.009	-0.060 ± 0.006	-0.022 ± 0.006	-0.007 ± 0.008	0.009 ± 0.006	-0.001 ± 0.006
2068	0.004 ± 0.005	-0.050 ± 0.006	-0.007 ± 0.007	0.011 ± 0.008	0.018 ± 0.005	-0.014 ± 0.006

the earlier analysis of Ref. [1]. Both analyses violated S -matrix unitarity. Our results for $\pi N \rightarrow \eta N$ differ significantly from those of Baker *et al.* [2]. Firstly, partial waves above G_{17} were not needed in the present analysis but that of Baker *et al.* included partial waves up to H_{19} . Also the D_{13} amplitude was found to be negligible over the entire energy range in the present work. Secondly, the S_{11} wave was poorly determined by Baker *et al.*, especially near the threshold region. This could be due to poor data but our prediction for the integrated cross section agrees satisfactorily with the precise and recent data from Prakhov *et al.* [10]. This re-enforces the reliability of the S_{11} amplitude from our analysis. The other partial waves where we disagree with Baker *et al.* are P_{13} and F_{15} at low energies. For the P_{11}

TABLE IV. Continued.

W (MeV)	G_{17}		G_{19}		H_{19}	
	Re(G_{17})	Im(G_{17})	Re(G_{19})	Im(G_{19})	Re(H_{19})	Im(H_{19})
1858	-0.002 ± 0.007	0.012 ± 0.006	-0.009 ± 0.007	-0.003 ± 0.005	0.003 ± 0.005	-0.011 ± 0.006
1888	0.006 ± 0.008	-0.001 ± 0.005	-0.003 ± 0.006	0.001 ± 0.007	-0.006 ± 0.006	-0.005 ± 0.005
1918	0.013 ± 0.005	0.003 ± 0.004	-0.016 ± 0.005	-0.002 ± 0.005	-0.007 ± 0.005	-0.003 ± 0.004
1948	0.008 ± 0.005	0.004 ± 0.004	-0.013 ± 0.004	-0.016 ± 0.005	-0.007 ± 0.005	0.009 ± 0.004
1978	-0.011 ± 0.007	0.023 ± 0.004	-0.000 ± 0.004	-0.009 ± 0.005	0.028 ± 0.005	-0.003 ± 0.006
2008	-0.002 ± 0.012	0.013 ± 0.008	-0.010 ± 0.007	-0.008 ± 0.008	0.021 ± 0.009	-0.018 ± 0.008
2038	-0.005 ± 0.007	0.009 ± 0.006	0.007 ± 0.005	-0.028 ± 0.006	0.005 ± 0.005	-0.002 ± 0.005
2068	-0.005 ± 0.005	-0.007 ± 0.004	0.001 ± 0.006	0.000 ± 0.006	0.010 ± 0.004	0.003 ± 0.003

amplitude, both Ref. [2] and the present work find significant contributions near 1700 MeV. The more recent 1995 analysis by Batanić *et al.* [16] used a three-channel unitary approach to obtain partial-wave amplitudes for $\pi N \rightarrow \pi N$ and $\pi N \rightarrow \eta N$, and to predict the same for $\eta N \rightarrow \eta N$. There is a striking resemblance of the S_{11} and P_{11} amplitudes between our analysis and one of the solutions in Ref. [16]. For higher partial waves, the differences are more pronounced. Also the analysis of Batanić *et al.* required the D_{13} and F_{17} amplitudes, which were not needed in the present work. Our analysis does better in describing the $\pi^- p \rightarrow \eta n$ differential cross section, especially at forward angles in the c.m. energy range 1650 to 2070 MeV, than either the 2008 EBAC analysis [19] based on a dynamical coupled-channels (DCC) model or the 2011 analysis [20] by the Jülich-Athens group based on the Jülich DCC model.

For $\pi^- p \rightarrow K^0 \Lambda$, the previous analyses [3–6] were also energy-dependent PWAs based on the simple parameterization $T = T_B + T_R$, which violates S -matrix unitarity. The 1970s analyses of $\pi^- p \rightarrow K^0 \Lambda$ by Knasel *et al.* [3], Baker *et al.* [2], and Saxon *et al.* [5] used differential cross section, polarization and/or polarized cross section data, but no spin-rotation data. The 1983 analysis by Bell *et al.* [6] included differential cross section and polarization data from their previous analyses [4, 5], plus spin-rotation data. Our results

broadly agree with these previous analyses, especially that by Bell *et al.* [6]. Their S_{11} amplitude has a similar behavior to ours except for an opposite over-all sign. The main difference is F_{15} is not required in Ref. [6] but is included in our work. The description of spin-rotation measurements by the present single-energy analysis is better in some cases than that by Bell *et al.* [6] and is as good as the recent work by the Bonn-Gatchina group [17]. Also the contributions we find for the leading partial waves (see Fig. 5) agree very well with the analysis by the Bonn-Gatchina group.

IV. SUMMARY AND CONCLUSIONS

We have extracted partial-wave amplitudes for $\pi N \rightarrow \eta N$ and $\pi N \rightarrow K\Lambda$ from a constrained single-energy analysis from threshold to a c.m. energy of 2.1 GeV. The contributing partial waves for $\pi N \rightarrow \eta N$ were found to be S_{11} , P_{11} , P_{13} , D_{15} , F_{15} , and G_{17} . For $\pi N \rightarrow K\Lambda$, S -, P -, and D -waves alone were sufficient to describe the differential cross section and polarization data but additional small partial waves (F_{15} , F_{17} , G_{17} , G_{19} , and H_{19}) were necessary to obtain a good fit of the spin-rotation data.

In conclusion, we have investigated $\pi N \rightarrow \eta N$ and $\pi N \rightarrow K\Lambda$ reactions through single-energy analyses constrained by a global unitary energy-dependent fit. Our results for $\pi N \rightarrow K\Lambda$ are mostly consistent with the analysis by Bell *et al.* [6] and with the Bonn-Gatchina analysis [17]. The inclusion of these amplitudes, in addition to πN , $\pi\pi N$, and γN into the global fit yields highly constrained information on resonance couplings. Also predictions of the integrated cross sections for $\pi^- p \rightarrow \eta n$ and $\pi^- p \rightarrow K^0\Lambda$ from the final global energy-dependent solution are in excellent agreement with the available data.

ACKNOWLEDGMENTS

This work was supported by the U.S. Department of Energy Grant No. DE-FG02-01ER41194. The authors thank the GWU group and especially Igor Strakovsky for providing part of the database for $\pi^- p \rightarrow \eta n$.

[1] J. Feltesse *et al.*, Nucl. Phys. B **93**, 242 (1975).

- [2] R.D. Baker *et al.*, Nucl. Phys. B **156**, 93 (1979).
- [3] T.M. Knasel *et al.*, Phys. Rev. D **11**, 1 (1975).
- [4] R.D. Baker *et al.*, Nucl. Phys. B **141**, 29 (1978).
- [5] D.H. Saxon *et al.*, Nucl. Phys. B **162**, 522 (1980).
- [6] K.W. Bell *et al.*, Nucl. Phys. B **222**, 389 (1983).
- [7] D.M. Manley and E.M. Saleski, Phys. Rev. D **45**, 4002 (1992).
- [8] R.A. Arndt, W.J. Briscoe, I.I. Strakovsky, and R.L. Workman, Phys. Rev. C **74**, 045205 (2006).
- [9] M. Shrestha, and D.M. Manley, to be submitted to Phys. Rev. C.
- [10] S. Prakhov *et al.*, Phys. Rev. C **72**, 015203 (2005).
- [11] N.C. Debehram *et al.*, Phys. Rev. D **12**, 2545 (1975).
- [12] W.B. Richards *et al.*, Phys. Rev. D **1**, 10 (1970).
- [13] W. Deinet *et al.*, Nucl. Phys. B **11**, 495 (1969).
- [14] R.M. Brown *et al.*, Nucl. Phys. B **153**, 89 (1979).
- [15] Orin I. Dahl, *et al.*, Phys. Rev. **163**, 1430 (1967).
- [16] M. Batinić *et al.*, Phys. Rev. C **51**, 2310 (1995).
- [17] A. Sarantsev, Sixth International Workshop on πN Partial-Wave Analysis, GWU, May 23 - 27, 2011- http://gwdac.phys.gwu.edu/pwa2011/Tuesday/sarantsev_PWA2011.pdf
- [18] A.V. Anisovich *et al.*, Eur. Phys. Jour. A **47**, 153 (2011).
- [19] J. Durand *et al.*, Phys. Rev. C **78**, 025204 (2008).
- [20] K. Nakayama *et al.*, J. Korean Phys. Soc. **59**, 224 - 246 (2011).

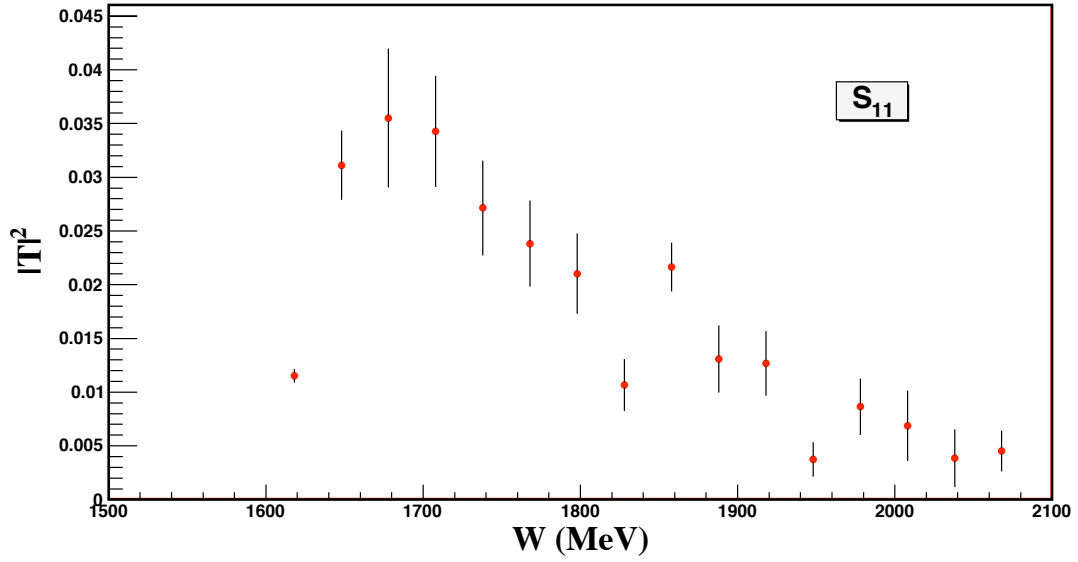


FIG. 1. $|T|^2$ vs. W for the $\pi^- p \rightarrow K^0 \Lambda$ S_{11} amplitude.

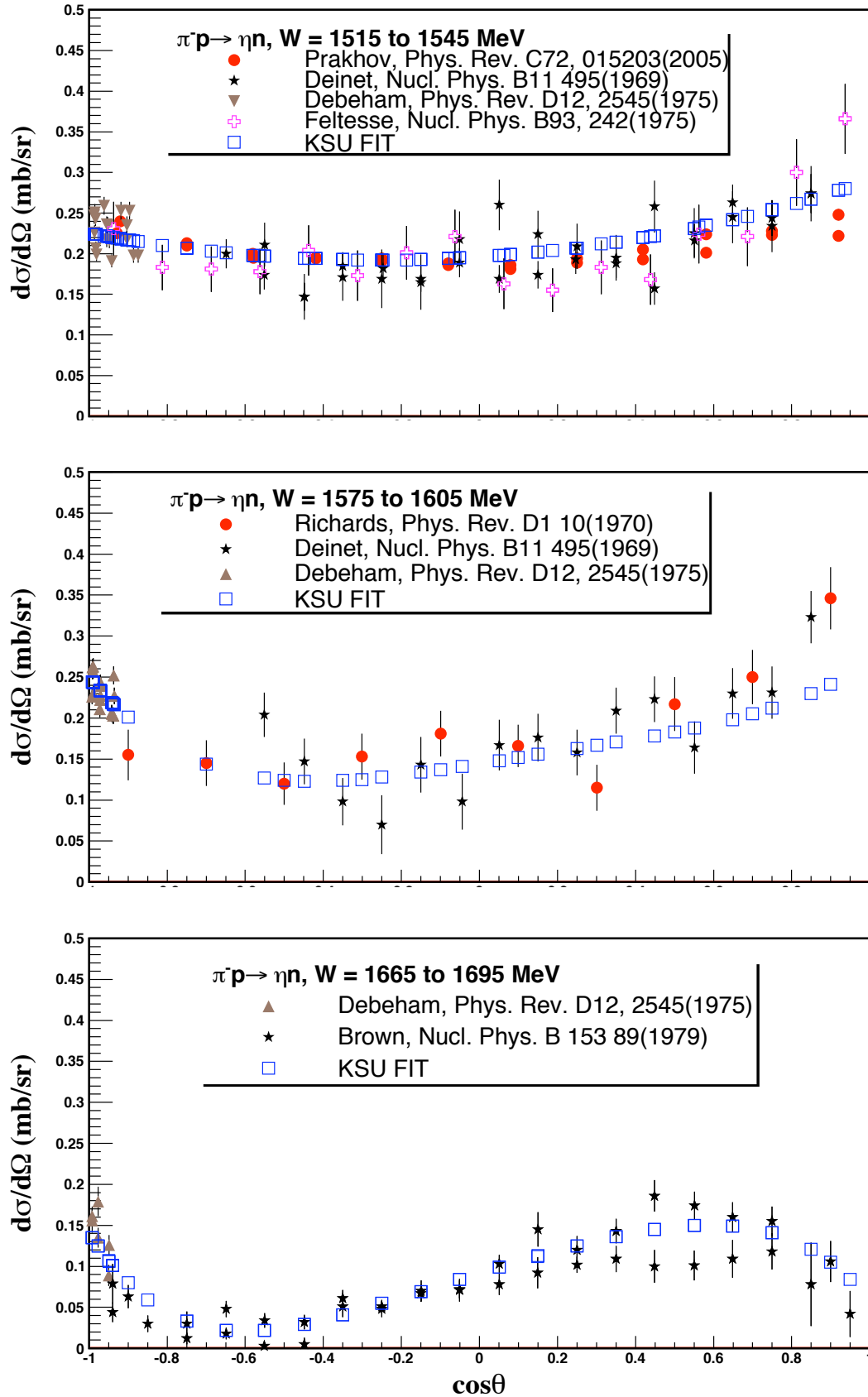


FIG. 2. Single-energy fit results for $\pi^- p \rightarrow \eta n$.

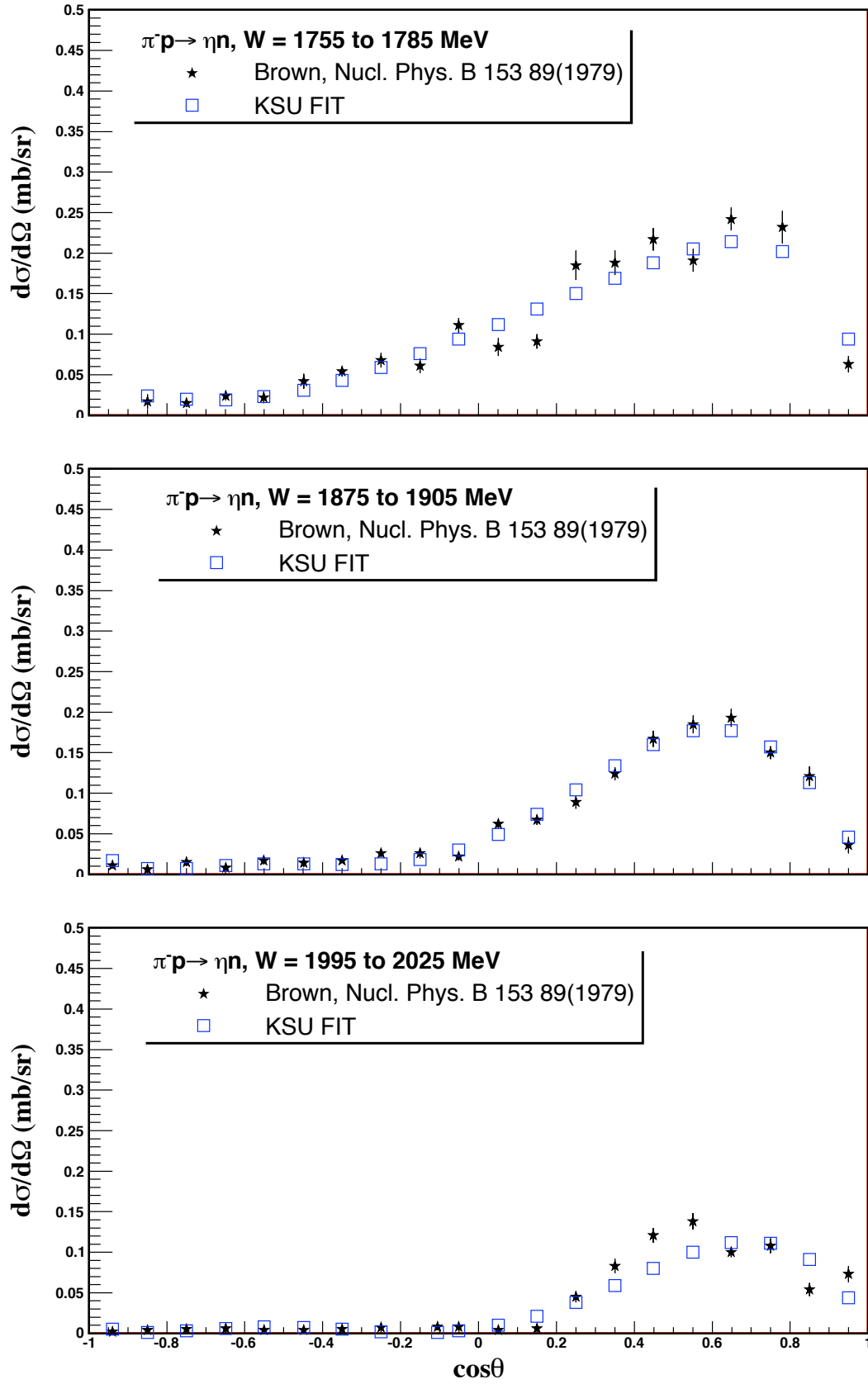


FIG. 2. (Cont'd)

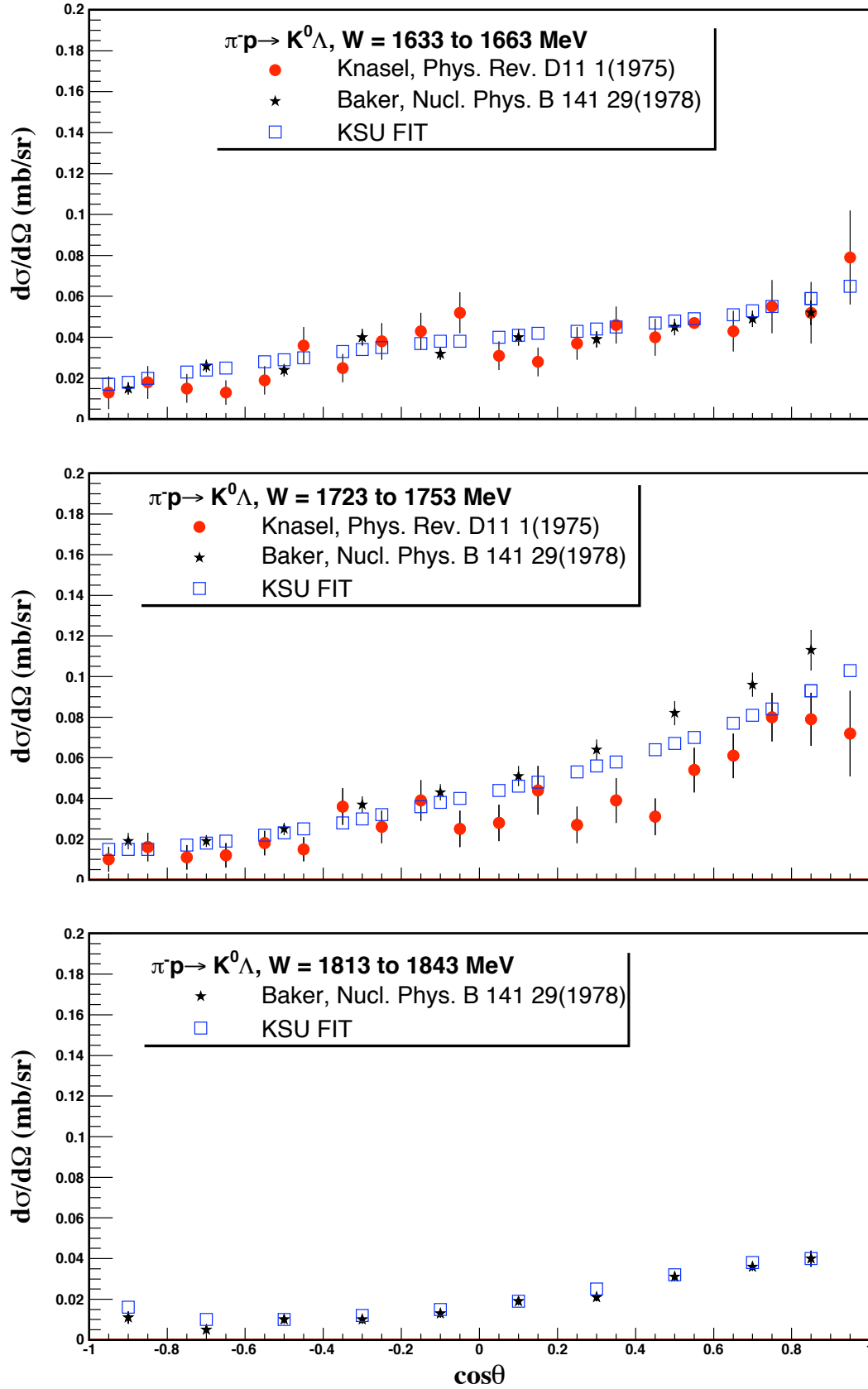


FIG. 3. Single-energy fit results for $\pi^- p \rightarrow K^0 \Lambda$.

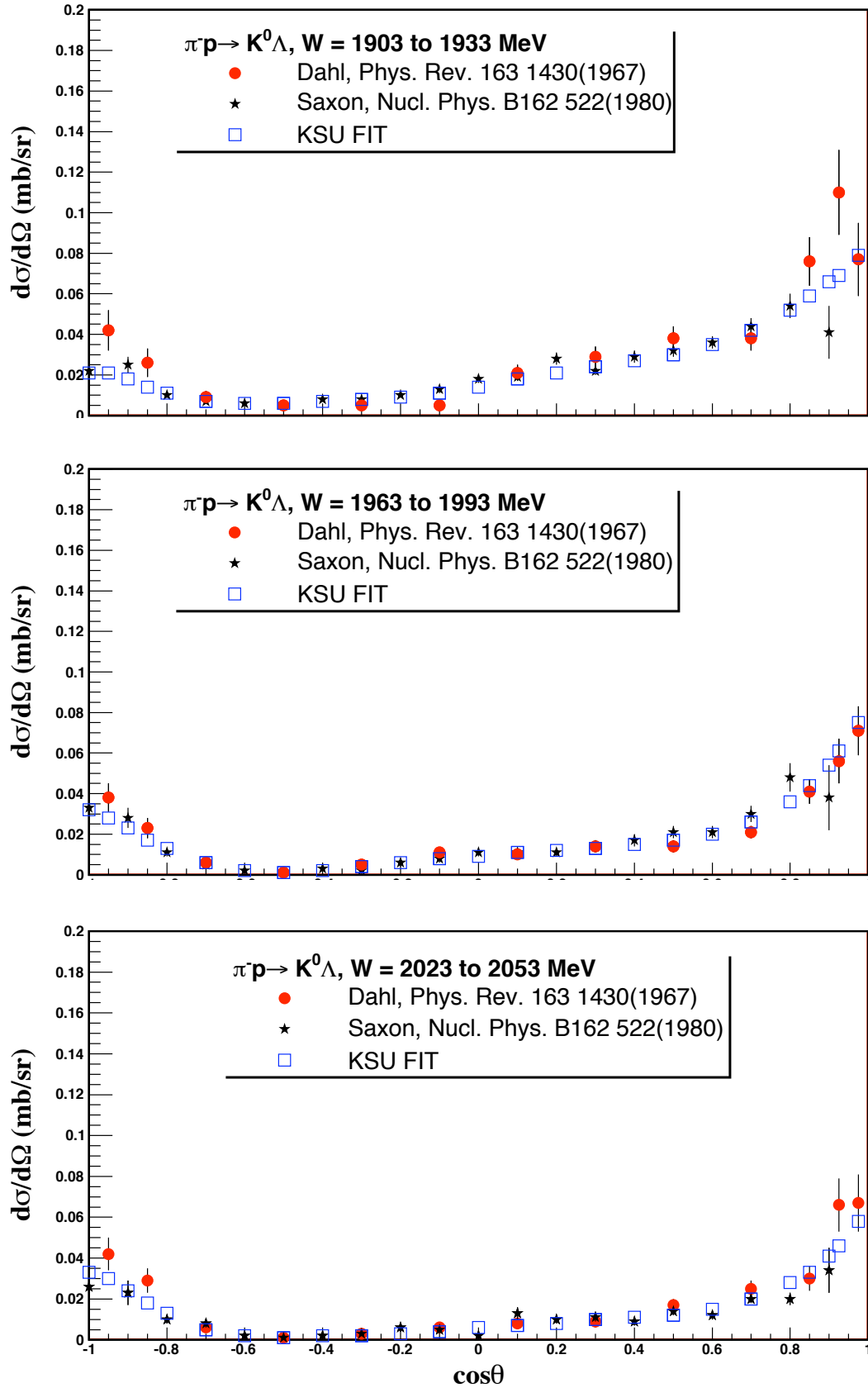


FIG. 3. (Cont'd)

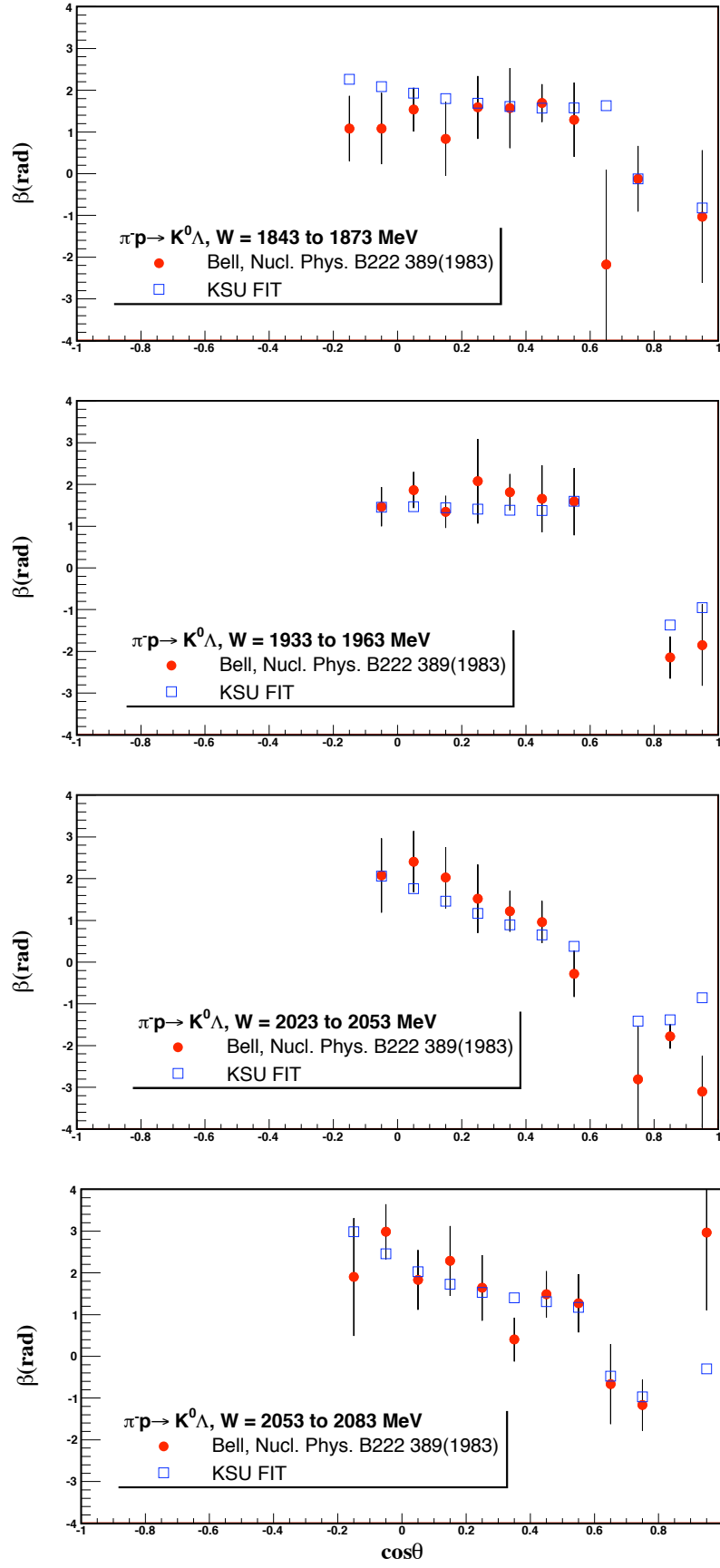


FIG. 4. Single-energy fit results for $\pi^- p \rightarrow K^0 \Lambda$.

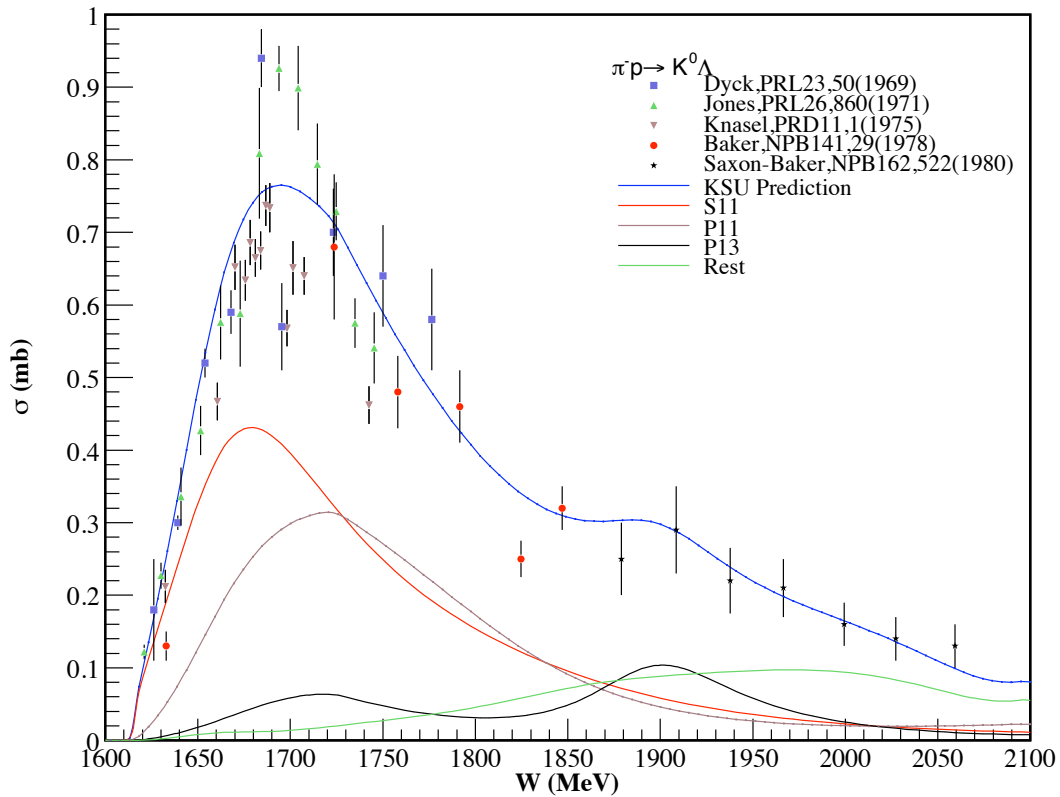
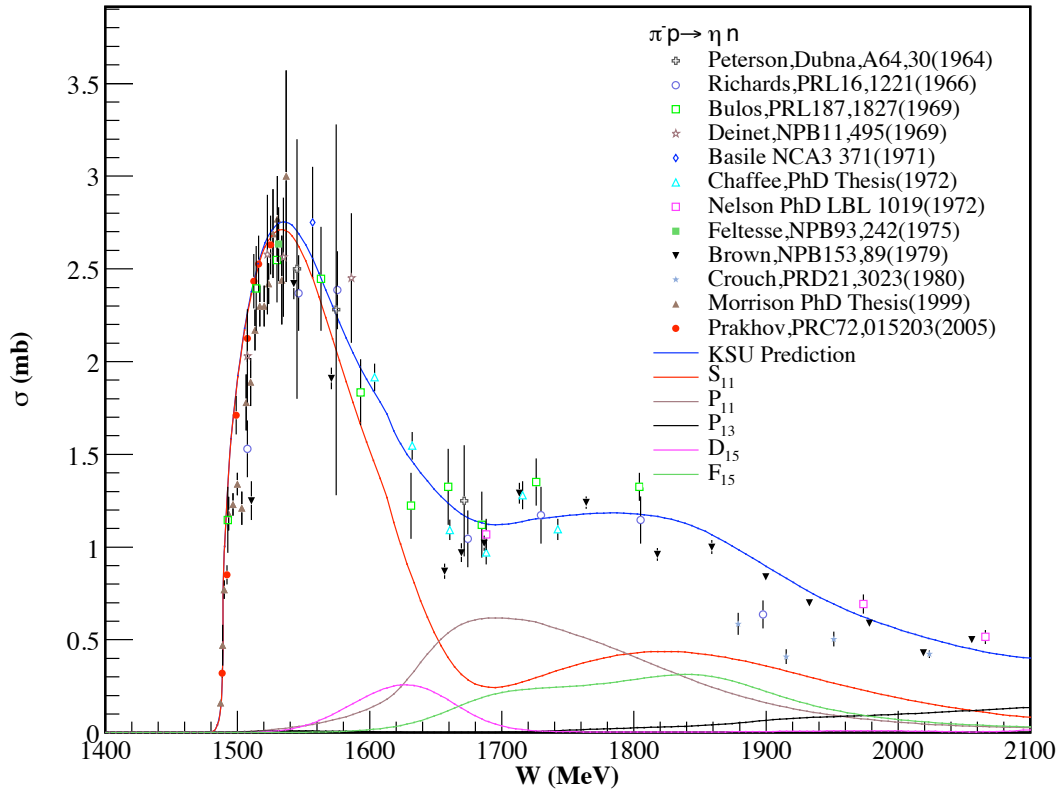


FIG. 5. Predictions of integrated cross sections of $\pi^- p \rightarrow \eta n$ and $\pi^- p \rightarrow K^0 \Lambda$.